Local Inhibition by 2-mercaptobenzothiazole of Early Stage Intergranular Corrosion of Copper

Sagar B Sharma, Vincent Maurice, Lorena H Klein, Philippe Marcus

Local Inhibition by 2-mercaptobenzothiazole of Early Stage Intergranular Corrosion of Copper

Journal of The Electrochemical Society, 2020 **167** 161504

Local Inhibition by 2-mercaptobenzothiazole of Early Stage Intergranular Corrosion of Copper

Sagar B. Sharma, Vincent Maurice,[z] Lorena H. Klein, and Philippe Marcus[*,z]

PSL University, CNRS—Chimie ParisTech, Institut de Recherche de Chimie Paris (IRCP), Physical Chemistry of Surfaces Group, 75005 Paris, France

Corrosion inhibition by 2-mercaptobenzothiazole (MBT) at the surface termination of various types of grain boundaries (GBs) was studied at the nanometer scale on microcrystalline copper in HCl acid solution using in situ electrochemical scanning tunneling microscopy (ECSTM). Macroscopic electrochemical analysis by cyclic voltammetry showed highly effective inhibition of Cu(I) active dissolution blocked by MBT pre-adsorption in a potential range of 0.15–0.2 V. ECSTM analysis of the initial stages of intergranular corrosion confirmed the mitigation of net intergranular dissolution by the pre-adsorbed MBT surface layer but also revealed the local accumulation of reaction products in the GB regions. For Coincidence Site Lattice boundaries other than coherent twins, intergranular dissolution, mitigated by the pre-adsorbed MBT layer, and protection by intergranular formation of a film of reaction products were observed. For random GBs, protection by reaction products was dominant, in agreement with their more reactive intrinsic character, generating more Cu(I) ions under anodic polarization and thus promoting the formation of a protective film of reaction products. Coherent twins did not show preferential intergranular reactivity compared to adjacent grains, indicating equally strong efficiency than on grains. These results bring new insight on how inhibition operates locally at various types of GBs.

 [DOI: 10.1149/1945-7111/abcc36]

Manuscript submitted October 13, 2020; revised manuscript received November 16, 2020. Published November 30, 2020. *This paper is part of the JES Focus Issue on Characterization of Corrosion Processes in Honor of Philippe Marcus.*

At the surface, polycrystalline metallic materials expose a grain boundary (GB) network to the environment, which can limit their durability because of intergranular corrosion. The degradation, localized at the GBs, initiates at the topmost surface before penetrating in the sub-surface, and eventually propagates to the entire GB network. Intergranular corrosion is known to relate to the GB character and GB energy from previous studies of GB engineered materials submitted to intergranular sub-surface penetrating attack.[1–21] Based on such knowledge, GB engineering aims at producing polycrystals having the most stable GB network, and thus mitigate their susceptibility to intergranular corrosion.

There are two main classes of GBs depending on their misorientation angle: i) low angle (<15°) GBs that can be described by a network of edge dislocations in the GB plane, and ii) high angle (>15°) GBs that do not obey such a crystallographic description and are more reactive because of their higher energy compared to low angle GBs. Among high angle GBs, those that can be described by a coincidence site lattice (CSL) are labeled Σn with 1/n defining the fraction of lattice sites shared by the two grains in the GB plane. The low Σ GBs, i.e. those with a high fraction of common lattice sites, have lower energies and are so-called "special" when they resist degradation as opposed to the high Σ ones, and the random high angle grain boundaries that cannot be described by a coincidence site lattice.[2,6,8,11–13,16] In *fcc* materials such as copper, Σ3 boundaries (also called twins) are most common and can resist intergranular sub-surface penetrating attack.[6,9,12,13,16] Depending on the specific orientation of their GB plane, Σ3 twins can be coherent or incoherent. It has been reported that only the Σ3 coherent twins (with a {111}-oriented GB plane) would better resist intergranular sub-surface penetrating attack.[3,13]

Improving our knowledge of intergranular corrosion also requires to investigate the initial stages of reaction, i.e. early intergranular corrosion, at the surface termination of grain boundaries before penetration in the sub-surface region and propagation. The alterations of the topmost surface of the metallic material must be characterized locally, with sufficient high space resolution, and preferably in situ and under electrochemical control in order to monitor the kinetics of the corrosion reaction. Recently, this has been achieved on microcrystalline copper using electrochemical scanning tunneling microscopy (ECSTM).[22–25] Dissolution in the active state,[22] as well as transient dissolution during passivation,[23,25] observed at the nanometer scale, were found weaker at the GB edges assigned to coherent twin boundaries than at other GB edges assigned to random or other CSL boundaries. Coupling with Electron Back-Scatter Diffraction (EBSD) characterization of the local GB character showed the susceptibility to early intergranular corrosion for high angle boundaries as well as Σ9 CSL boundaries. For Σ3 coherent twins, the behavior was found dependent on the deviation angle of the GB plane from the exact orientation with a transition from resistance to susceptibility between 1° and 1.7° of deviation.[26]

The use of corrosion inhibitors has been proven to be an effective approach to mitigate the corrosion of metals and alloys in contact with aggressive environments. Azole derivatives such as 2-mercaptobenzothiazole (MBT, $C_7H_5NS_2$) are often used as corrosion inhibitors for copper or its alloys.[27–41] MBT has been reported to have a remarkable efficiency under neutral saline, acid and alkaline conditions[27,28,30,32,37–40] and to act as a mixed-type inhibitor.[29,37,42] There are two sulfur atoms and one nitrogen atom in the MBT molecule, that can, concomitantly or individually, strongly bond to copper atoms and thus enable chemisorption to form a stable molecular film protecting the copper surface from corrosion.[30,36,37,40,43–48] The formation of a Cu-MBT film has been proposed[27,28] and the film thickness would depend on pH with only a monolayer film forming in the range of Cu_2O stability (pH > 4) whereas multilayers would form in the range of Cu_2O instability (pH < 3).[27] The mechanism would consist of a surface reaction of Cu(I) ions with pre-adsorbed MBT, and not of a complex precipitated from the solution.[29] If pre-adsorbed on a copper surface in the metallic state, MBT forms a monolayer that prevents oxide formation as observed in alkaline aqueous solution[40] and in the gas phase.[44–46]

Here, we report on the nanoscale local characterization using electrochemical scanning tunneling microscopy (ECSTM) of the inhibition of early intergranular corrosion of copper by MBT in HCl acid solution in which no stable copper oxide is formed. Despite the well-established corrosion inhibition properties of MBT and other inhibitors on polycrystalline copper, there are, to the best of our knowledge, no studies on the local aspect of early stage intergranular corrosion in the presence of inhibitors and the mechanisms of

*Electrochemical Society Fellow.
[z]E-mail: vincent.maurice@chimie-paristech.fr; philippe.marcus@chimie-paristech.fr

inhibition at the surface termination of grain boundaries. The results reported here bring new insight on the inhibition process at various types of GBs.

Experimental

Microcrystalline copper samples were used.[19,22–26,49,50] They were obtained from high-purity cast electrolytic tough pitch copper, (ETP-) Cu, by cryogenic rolling after freezing in liquid nitrogen. Annealing was limited to 1 min at 200 °C to ensure full recrystallization while preserving a GB network of suitable cell size for the relatively small STM field of view, as confirmed by electron backscattered diffraction (EBSD)[22,23] and the data presented hereafter. No preferential grain orientation, i.e. a nearly random texture, was obtained[23] and 66% of the GB length corresponded to Σ3 CSL boundaries, the other 34% being random boundaries for the most part.[22,23] Samples were mechanically polished with diamond spray down to a final grade of 0.25 μm for surface preparation, which was followed by electrochemical polishing in 66% orthophosphoric acid at 3 V vs a copper counter electrode for 15 s in order to remove the cold work layer.

ECSTM analysis was performed with an Agilent Technologies system (PicoSPM base, Keysight STM S scanner, PicoScan 2100 controller, PicoStat bi-potentiostat and Picoscan software). The homemade ECSTM cell is made of Kel-F and contains ~350 μl of electrolyte. The working electrode area is 0.16 cm^2 delimited using a VITON® O-ring. Two Pt wires served as counter electrode and pseudo reference electrode (+0.20 V SHE). ECSTM cell cleaning and tip preparation have been detailed elsewhere.[51–55]

A non-deaerated 10 mM HCl(aq) aqueous acid solution (pH 2) was used as electrolyte, prepared from ultrapure HCl and Millipore water (resistivity > 18 MΩ cm). MBT was added at a concentration of 0.1 mM obtained by dissolution from the powder physical state. In order to avoid any uncontrolled corrosion, the samples were exposed to the electrolyte at −0.45 V SHE, i.e. below the open-circuit potential value of −0.35 V/SHE. Then, a cathodic reduction pre-treatment was applied in order to reduce the native oxide film. The potential was repeatedly cycled (0.2 V s^{-1}) down to −0.60 V SHE at the onset of hydrogen evolution and backward to the value of −0.45 V/SHE until the cyclic voltammograms (CVs) showed no cathodic peak associated with Cu(I) to Cu(0) reduction. Two cycles were enough to fully reduce the native oxide formed after electropolishing.

After this pre-treatment, ECSTM images of the microcrystalline copper surface in the metallic state were taken at −0.45 V/SHE for localization of grain boundaries of interest. Afterwards, anodic oxidation was forced by cycling (1 mV s^{-1}) the potential first up to the anodic apex of −0.18 V SHE then backward to the cathodic apex of −0.60 V SHE and finally upward to the initial value of −0.45 V/SHE. This cycle was repeated up to 4 times and new ECSTM images of the surface were taken at −0.45 V/SHE after 2 and 4 cycles. During electrochemical treatment, the STM tip was kept engaged but not scanning the surface, so as to keep the area of interest in the STM field of view after cycling. The evolution of the local topography could thus be followed after electrochemical cycling. The ECSTM images were acquired in the constant current mode. No filtering was used and the recorded images were processed with the Gwyddion software.[56]

Line profile analysis was applied to measure the topography across the GB regions. The line profiles were obtained by averaging 30 adjacent line scans drawn across the grain boundary, covering a local distance of ~170 nm along the boundary.[24,26] The GB depth was measured as the local difference in topographic height between the bottom of the GB regions and the surface level of the grains directly above. Ten different measurements were performed for each selected site and the reported error bar is the standard deviation for these ten measurements.

Results and Discussion

Macroscopic electrochemical behavior.—Figure 1 shows the effect of MBT on the electrochemical behavior of copper in 10 mM HCl(aq) as characterized by cyclic voltammetry. The CV measurements characterize the macroscopic electrochemical response of the surface. When showing substantial activity, this response can be assigned essentially to the reactivity of the grains since the exposed surface fraction of the GB network is very small compared to that of the grains, as confirmed by the ECSTM images presented below. In contrast, if only residual activity is observed, it corresponds to the sites of preferential reactivity, and thus emphasizes the response of the exposed GB network.

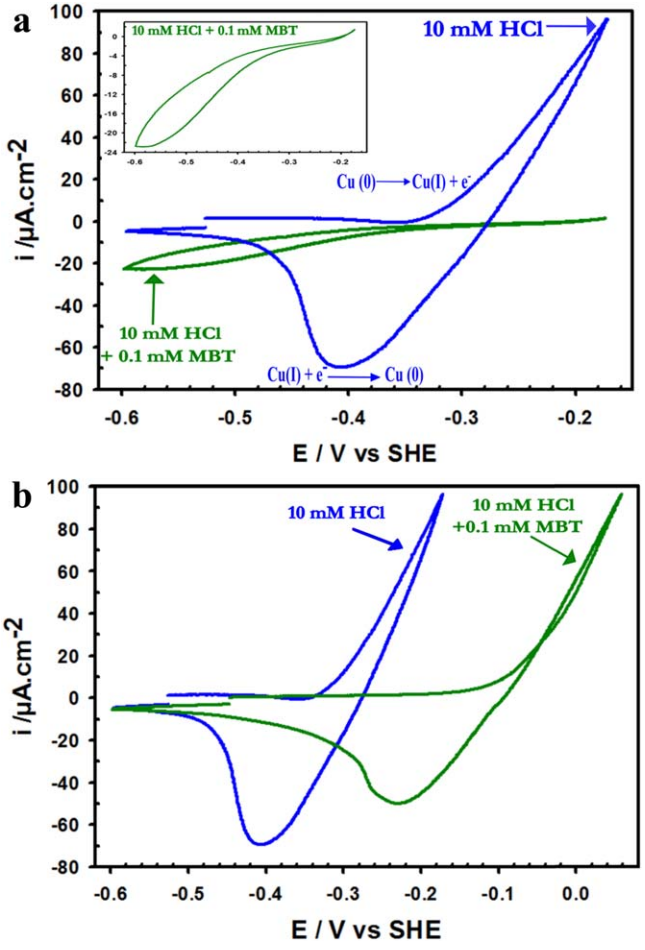

Figure 1. Cyclic voltammograms in the ECTM cell for microcrystalline copper in 10 mM HCl(aq), first cycle, scan rate = 1 mV s^{-1}: (a) CVs recorded without and with 0.1 mM MBT in the solution until anodic apex of −0.18 V. Inset shows enlarged CV obtained in the presence of MBT. (b) CVs recorded without and with 0.1 mM MBT in the solution until an anodic apex corresponding to the anodic current of 100 μA.cm^{-2}.

Figure 1a shows the CVs obtained after reduction of the native oxide and starting at −0.45 V/SHE in the metallic state (first cycle is shown). In the absence of MBT, the increase of the anodic current for E > −0.35 V/SHE is assigned to the anodic oxidation of copper ($Cu(0) \rightarrow Cu(I) + e^-$). No stable copper oxide is formed at pH 2 and the Cu(I) ions formed in this potential range dissolve as $CuCl_2^-$ in HCl medium.[57–60] In the reverse scan, a cathodic peak is observed like in previous studies.[26,60–65] It is assigned to the reductive deposition of dissolved Cu(I) and observed in the present experimental conditions at −0.40 V SHE.

The integration of the positive current density measured during the anodic and reverse cathodic scans yields a total value of the anodic charge density transfer of 26 885 μC cm^{-2}. This charge transfer amounts to an equivalent thickness δ of reacting copper of 19.7 nm as calculated using Eq. 1,

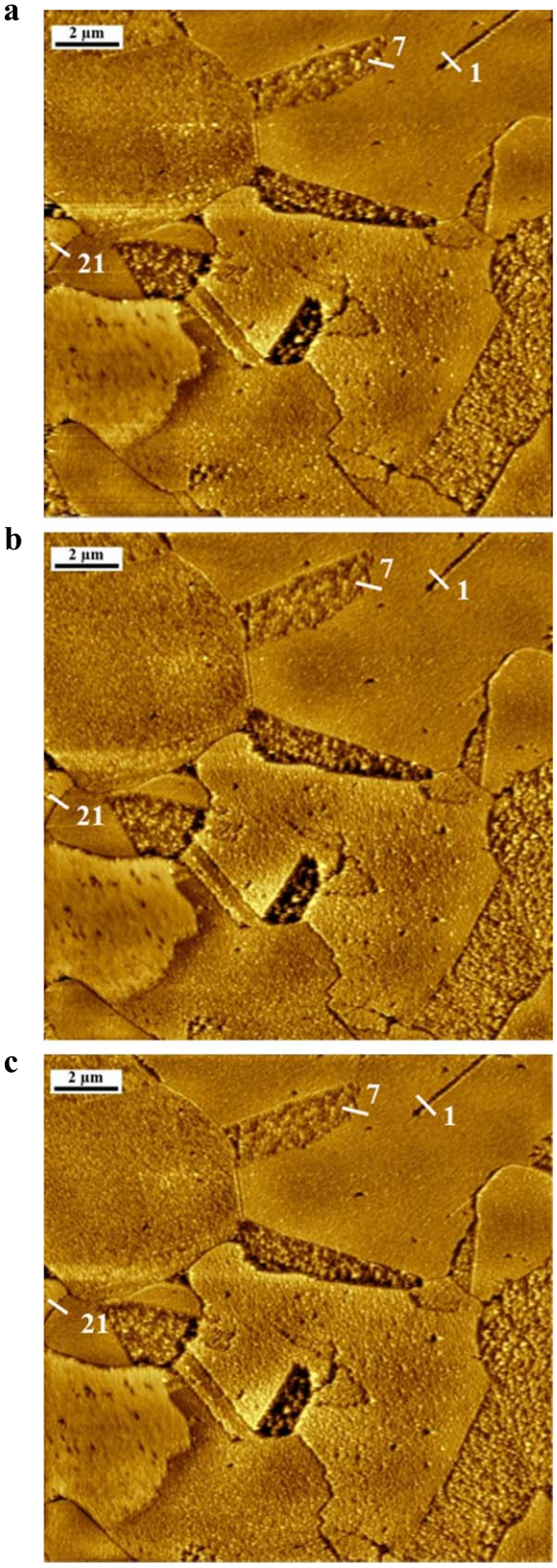

Figure 2. Topographic ECSTM images of microcrystalline copper as obtained in situ at −U = 0.45 V/SHE before and after cycling in 10 mM HCl(aq) + 0.1 mM MBT (Z range ΔZ = 7 nm, tip potential U_{tip} = −0.8 V SHE, tunneling current I_t = 1 nA): (a) Initial surface state; (b) Surface state after 2 CVs; (c) Surface state after 4 CVs.

$$\delta = \frac{qV_m}{zF} \quad [1]$$

where q is the charge density, V_m the molar volume of metallic copper (7.1 cm^3 mol^{-1}), z the number of exchanged electrons (1), and F the Faraday constant. This value of 19.7 nm corresponds to 95 equivalent monolayers (ML) of copper being dissolved since one (111)-oriented ML of copper is 0.208 nm thick from the bulk *fcc* structure. A 3-dimensional (3D) volume of material was thus consumed by the dissolution reaction in these testing conditions. The cathodic charge density transfer measured during the cathodic scan is 22 007 μC cm^{-2}, lower than the anodic one and indicating that about ∼17 ml of copper irreversibly dissolved during the CV treatment.

In the presence of MBT, the CV is nearly completely flat until the anodic apex (Fig. 1a), showing highly efficient inhibition of the dissolution of copper. In our testing conditions, MBT pre-adsorbs on copper covered by the native oxide and the reduction process of the native oxide occurs in the presence of a surface layer of MBT. As a result, the Cu atoms dissociated from oxygen by electro-reduction may be captured by the molecular surface layer, and it can be expected that the MBT film pre-formed in these conditions includes copper. The enlarged CV is shown in the inset. The increase of the anodic current is shifted anodically indicating that the anodic oxidation of copper and atomic transport across the interface requires a higher driving force. At the anodic apex, the current is much lower due to the barrier effect of the pre-adsorbed MBT molecular layer. In the reverse scan, no cathodic peak is observed in the range of −0.3 to −0.50 V/SHE unlike in the absence of the inhibitor. This is consistent with the MBT pre-formed surface layer blocking dissolution in these conditions of anodic polarization, and thus the subsequent reductive deposition of copper.

Figure 1b shows the first CV obtained when increasing anodic polarization potential in the presence of MBT. For E > −0.20 to −0.15 V/SHE, the anodic current increases continuously until the anodic apex and a cathodic peak is observed in the reverse scan. Like in the absence of MBT, this behavior indicates a regime of anodic dissolution followed by reductive redeposition of dissolved copper upon reverse polarization. The anodic shift of the regime of anodic dissolution confirms that the MBT pre-adsorbed layer inhibits dissolution by a barrier effect in a potential window of about 0.15–0.2 V. However, this barrier effect does not resist the further increase of the driving force for Cu dissolution. The results obtained in this range of anodic polarization do not support the view that the reacting copper atoms could be directly captured by the pre-adsorbed MBT surface layer to form a protective Cu(I)-MBT film by a surface reaction,[29] since a dissolution/redeposition behavior is observed like at lower potential in the absence of MBT as seen in Fig. 1b. However, the previously proposed formation of a Cu-containing film[27,28] by redeposition from the solution cannot be excluded.

In the presence of MBT, the anodic charge density transfer cumulated until the anodic apex of −0.18 V SHE and in the reverse scan is 36 μC cm^{-2}. This corresponds to only 0.03 nm (0.13 ml) of copper having reacted to be compared with 19.7 nm (95 ml) without MBT, showing extremely high anodic inhibition efficiency (99.9%) in these test conditions. The residual anodic activity observed at the apex of −0.18 V/SHE likely occurrs at the most reactive surface sites, and thus at the emergence of the grain boundaries while the grain surfaces remain better protected. Hereafter, we discuss the ECSTM data obtained in the presence of the MBT inhibitor in these conditions of low residual activity generated at the apex of −0.18 V/SHE. The ECSTM data obtained in similar conditions of residual activity in MBT-free 1 mM HCl solution were discussed previously.[22,26]

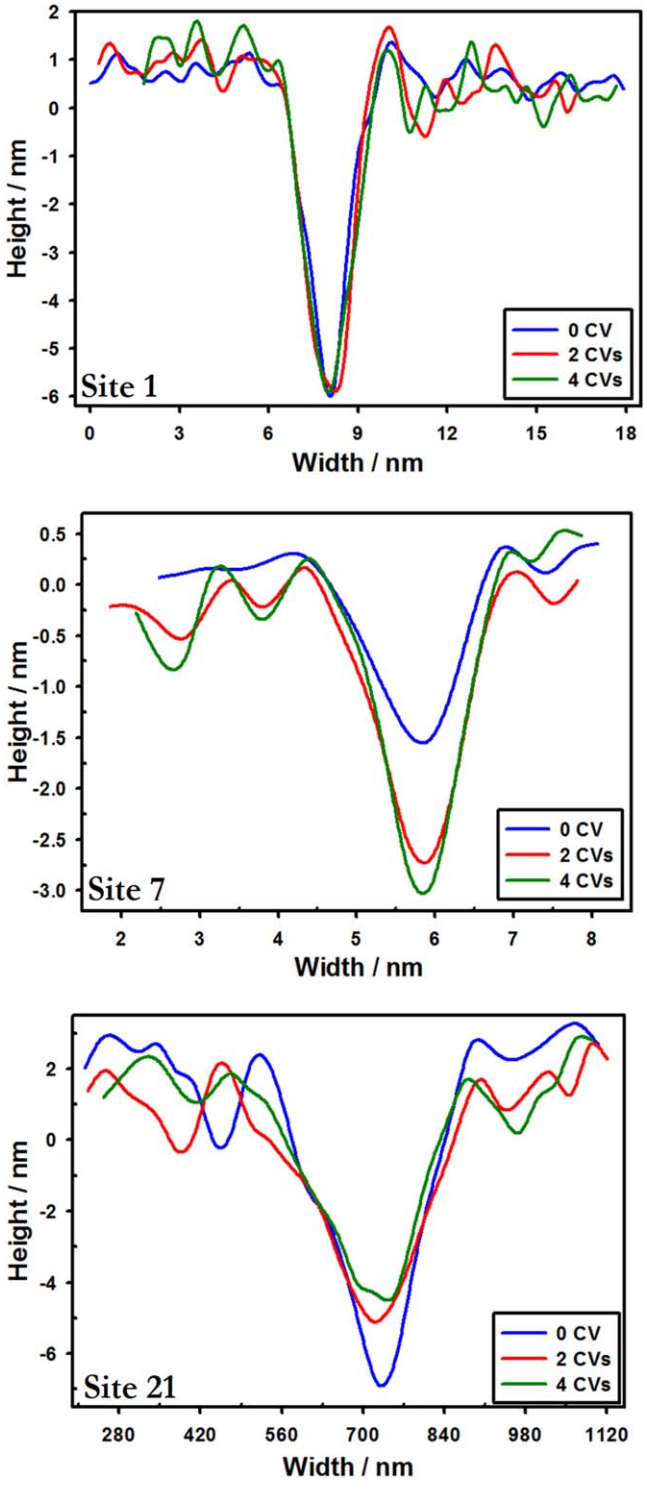

Figure 3. Average topographic line profiles measured across the GB at sites #1, 7 and 21 in Fig. 2.

MBT inhibition effects on early stage intergranular corrosion.—Figure 2 shows a typical local area at the topmost surface of microcrystalline copper where the microstructure could be repeatedly imaged in situ by ECSTM before (Fig. 2a) and after 2 (Fig. 2b) and 4 (Fig. 2c) CVs in the 10 mM HCl(aq) + 0.1 mM MBT solution. In this area of interest, the microstructure exposes grains and subgrains. Some of the grains are measured at a lower topographic height, which is attributed to differences of local surface reactivity during surface preparation by electrochemical polishing (etching) and subsequent in situ reduction of the native oxide film. The GB edges, i.e. the termination of the GB planes, and their immediate vicinity, hereafter referred to as the GB regions, are also well marked by the surface preparation. Some GB regions are measured lower, also as a result of higher local surface reactivity revealed by surface preparation while others can be located thanks to topography variations between the adjacent grains.

Based on our previous work,[22,24–26] the different types of observed grains boundaries were assigned according to the GB morphology in the surface plane. Two parallel GBs separating a sub-grain is a configuration typical of Σ3 coherent twins (with a {111}-oriented GB plane). Short and straight GBs are assigned to low Σ CSL boundaries, including Σ3 incoherent twins. Straight segments observed along a GB of locally straight or curved morphology are assigned to high Σ CSL boundaries. Curved GBs are assigned to random boundaries.

In total, 43 local sites were identified at which the depth at the bottom of the GB region could be geometrically measured with this procedure before and after 2 and 4 CV cycles. Typical examples are shown in Fig. 3 for sites 1, 7 and 21 in Fig. 2. Comparative analysis of the variations of the GB depth in this population of 43 sites revealed five types of local intergranular behavior after 2 and 4 CVs: i) no variation of the GB depth, ii) repeated increase, iii) repeated decrease, iv) decrease followed by increase, and v) increase followed by decrease.

There were five sites, labelled 1 to 5 in Fig. 4a, at which no net variation of the depth of the GB region was measured after 2 and 4 CVs. The depth measured across all five sites is different due to differences of local surface reactivity during surface preparation. The bar graph in Fig. 4b shows no significant increase nor decrease of the depth of the GB region that would characterize a different behavior than on the adjacent grains caused by intergranular corrosion. In the absence of inhibitors, this intergranular corrosion resistant behavior is typical of Σ3 coherent twins like characterized in testing conditions of sub-surface penetrating attack[3,13] and like also observed by in situ ECSTM measurements of early intergranular corrosion.[22,26] Here, it is observed for sites 1 and 2 which are located along two parallel GBs separating a sub-grain, a configuration typical of Σ3 coherent twins. Thus, the absence of preferential local reactivity in these sites cases can be assigned to the intrinsic resistance of the Σ3 coherent twins rather than to the presence of the MBT inhibitor. This locally resistant intergranular behavior is also observed for sites 3 to 5. Site 3 is located at a short and straight boundary assigned to a low Σ CSL boundary. Sites 4 and 5 are located along straight segments of GBs assigned to high Σ CSLs. In these local sites, which would be attacked without inhibitor,[22,26] the pre-adsorbed MBT layer provides equal protection to the GB region than to the adjacent grains, like schematically illustrated in Fig. 5a.

For thirteen sites, labelled 6 to 18 in Fig. 4a, a net increase of the depth of the GB region could be measured after 2 and 4 CVs (Fig. 4c). The increase of the GB depth is indicative of the preferential local consumption of the material by irreversible and faster dissolution than on the adjacent grains. It has been previously observed for early intergranular corrosion of copper in 1 mM HCl (aq) solution without inhibitor with an amplitude of the increase of the GB depth not exceeding 2 nm.[26] In the present work performed in more acidic 10 mM HCl(aq) + 0.1 mM MBT, it was observed with a maximum amplitude reaching 3 nm, which is assigned to the effect of MBT mitigating, but not fully blocking, preferential dissolution at the less resistive GBs because of less efficient MBT protection than on the adjacent grains (Fig. 5b). Among the sites where this imperfect MBT protection is observed, sites 8–10 and 15 are located along straight GB segments assigned to high Σ CSLs. For these high Σ CSL boundaries, local intergranular irreversible dissolution is observed but mitigated by the MBT surface layer given the relatively small increase of the GB depth. Sites 6, 7, 11–14, 16–18 belong to curved GBs or GB segments assigned to random boundaries. Note that the highest amplitude of the GB depth increase resulting from the imperfect MBT protection is measured at site 6 assigned to a random GB.

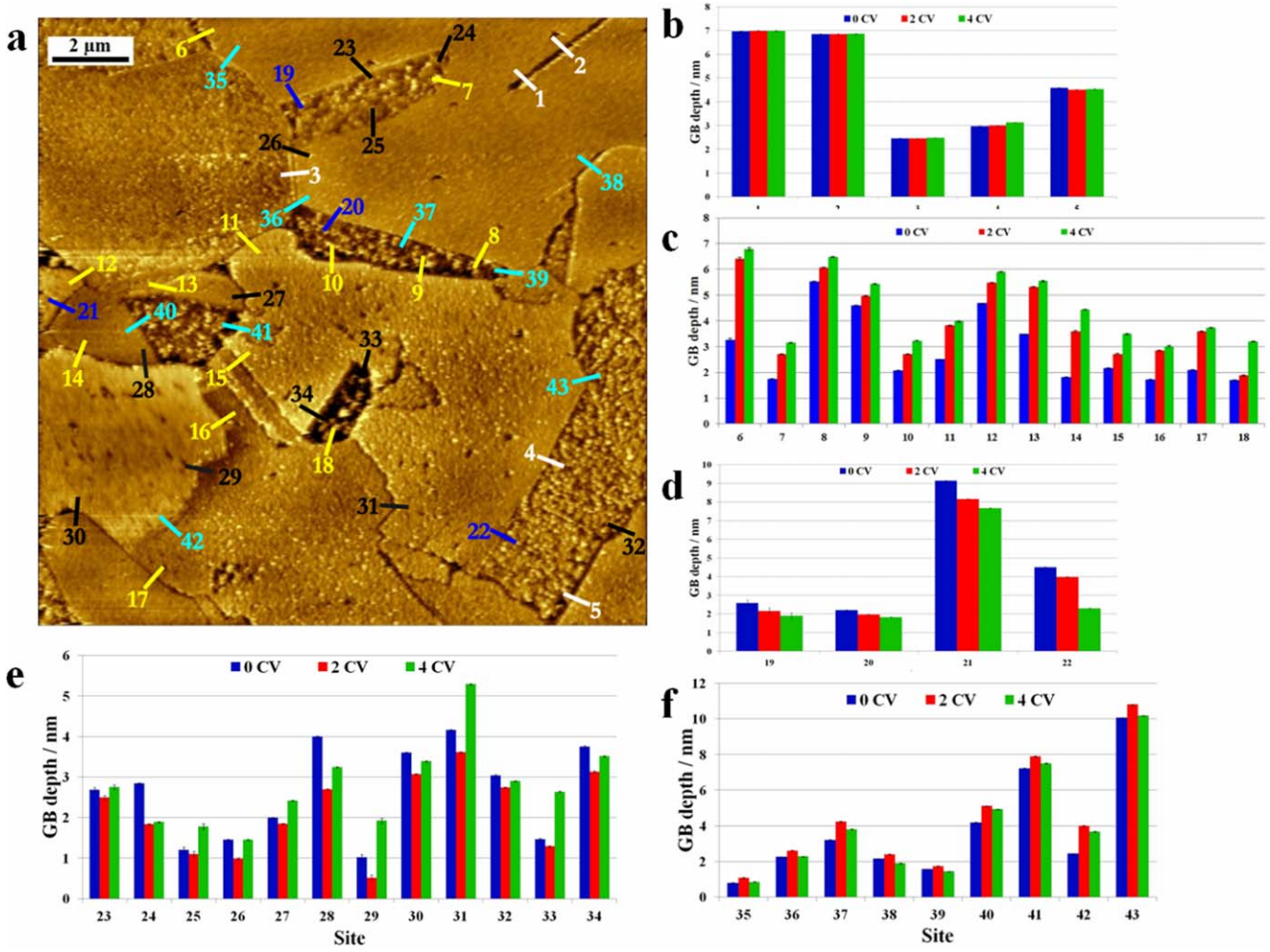

Figure 4. Identification of early stage intergranular corrosion behavior of microcrystalline copper sites in 10 mM HCl(aq) + 0.1 mM MBT: (a) Topographic ECSTM image with grain boundary sites labelled 1 to 43; (b) Bar graph of the depth measured across the GB sites (labelled in white in (a)) showing no preferential reactivity after 2 and 4 CVs; (c) Bar graph of the GB sites (labelled in yellow in (a)) showing depth increase after 2 and 4 CVs; (d) Bar graph of the GB sites (labelled in dark blue in (a)) showing depth decrease after 2 and 4 CVs; (e) Bar graph of the GB sites (labelled in black in (a)) showing depth decrease and subsequent increase after 2 and 4 CVs, respectively. (f) Bar graph of the GB sites (labelled in light blue in (a)) showing depth increase and subsequent decrease after 2 and 4 CVs, respectively.

The four sites labelled 19 to 22 in Fig. 4a are those at which a net decrease of the depth of the GB region could be measured after 2 and 4 CVs (Fig. 4d). The decrease of the GB depth is indicative of a local accumulation of reaction products, more important in the GB region than on the adjacent grains. It has been observed in previous ECSTM studies of passivation of copper in 0.1 M NaOH(aq) and attributed to the formation of the Cu(I) passive oxide film locally thicker in the GB regions than on the adjacent grains.[24,25,66] In 10 mM HCl(aq) + 0.1 mM MBT, the electrochemical response does not show a passivation-like behavior of the grains in the potential range tested but only a displaced onset of anodic oxidation. However the anodic oxidation could preferentially occur in the GB regions because of their higher reactivity, generating locally more Cu(I) ions and thus leading to the local growth of a layer of reaction products, possibly Cu(I)-MBT species,[27,28] protecting more efficiently against anodic dissolution than the MBT film formed by pre-adsorption. No such layer would form on the less reactive adjacent grains (Fig. 5c). The growth process would be repeated at each treatment cycle thus leading to an increased thickness of the film formed in the GB region. This local formation of a film of reaction products is observed at sites 19, 20 and 22 along straight GB segments assigned to high Σ CSL boundaries. It is also observed at site 21 along a random GB characterized by a curved morphology.

For the twelve sites labelled 23 to 34 in Fig. 4a, the behavior was first characterized by a decrease of the GB depth after 2 CVs and subsequently by an increase after 4 CVs (Fig. 4e). These variations can be small (e.g. site 23) or more pronounced (e.g. site 31). Like for sites 19 to 22, the decrease of the GB depth measured after 2 CVs is indicative of the preferential accumulation in the GB region of reaction products that leads to the formation of a film mitigating, at least temporarily, preferential dissolution in the GB region. However, this protective effect does not persist since after 2 more CVs the GB depth increases due to dissolution (Fig. 5d). This unstable behavior suggests transient protection provided by the local film initially formed and likely altered during the subsequent CV treatments. Among the GB sites where this behavior is observed, sites 23 and 34 belong to straight GB segments assigned to high Σ CSLs. Note that at these two sites the GB depth variations are small indicating little alterations of the local early intergranular corrosion behavior. All the other sites belong to curved or locally curved boundaries assigned to random boundaries. Half of them (25, 27, 29, 31 and 33) show an increase of the GB depth after 4 CVs to a value higher that the initial value measured before cycling, indicating a pronounced alteration of the transient protection against anodic dissolution brought by the initial growth of the surface film of reaction products.

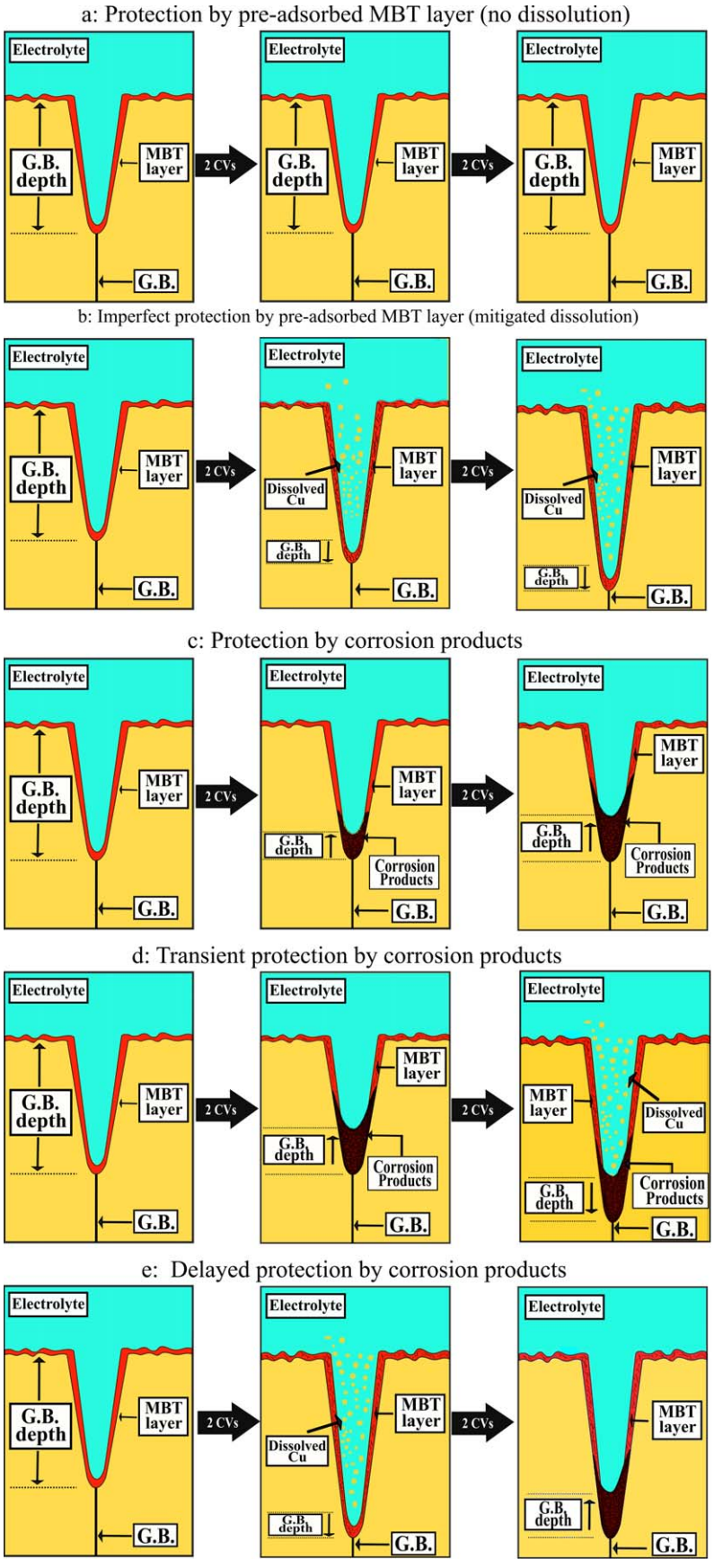

Figure 5. Schematic illustration of observed MBT inhibiting effects on early intergranular corrosion of copper in acid electrolyte.

Table I. Observed occurrences of each type intergranular corrosion behavior for various types of grain boundaries for microcrystalline copper in 10 mM HCl(aq) + 0.1 mM MBT.

Intergranular behavior	CTs	Low Σ CSLs	High Σ CSLs	Random GBs
Resistance (intrinsic)	2	—	—	—
Protection by pre-adsorbed MBT layer (no dissolution)	—	1	2	—
Imperfect protection by pre-adsorbed MBT layer (mitigated dissolution)	—	—	4	9
Protection by corrosion products	—	—	3	1
Transient protection by corrosion products	—	—	2	10
Delayed protection by corrosion products	—	—	3	6

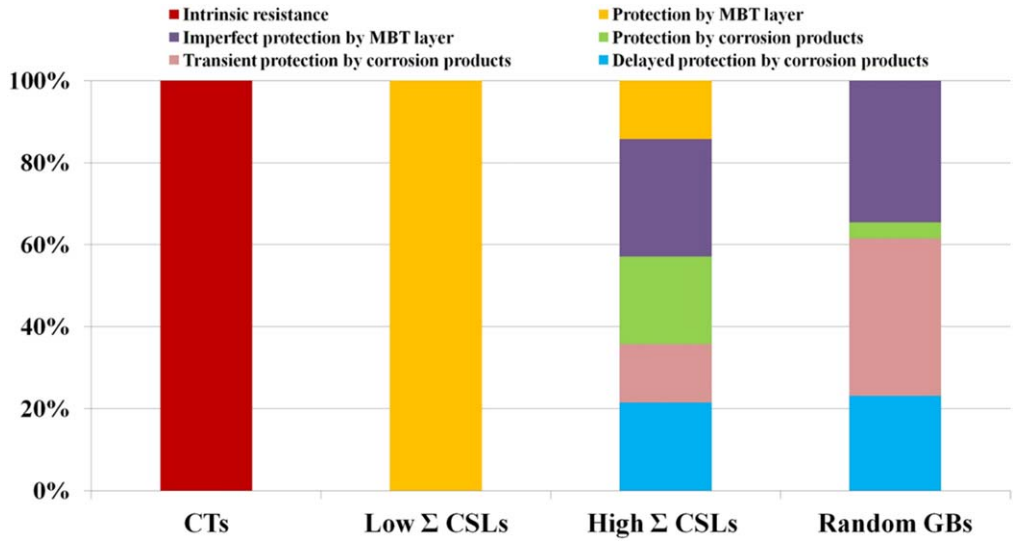

Figure 6. Percentage of each type of intergranular corrosion behavior observed on various types of grain boundaries for microcrystalline copper in 10 mM HCl (aq) + 0.1 mM MBT.

Labels 35 to 43 in Fig. 4a correspond to the nine sites at which the behavior was first characterized by an increase of the GB depth after 2 CVs and subsequently by a decrease after 4 CVs (Fig. 4f). Like for sites 6 to 18, the increase of the GB depth measured after 2 CVs is indicative of intergranular net dissolution. Mitigation by the MBT is supported by the relatively small increase of the GB depth reaching 1 nm at the most, less than in the less aggressive 1 mM HCl (aq) solution in the absence of MBT.[26] However, after 2 more CVs, the local accumulation of reaction products decreases the GB depth with formation of a protective film against dissolution. In this case, the repeated alterations of the MBT surface layer brought by the CV treatment promote the delayed formation of a protecting film in the GB regions (Fig. 5e). Three sites (37, 38 and 40) at which this behavior is observed belong to straight GB segments assigned to high Σ CSLs. The other six sites (35, 36, 39, 41–43) belong to curved or locally curved boundaries assigned to random GBs.

Intergranular inhibiting effects according to GB type.—Table I and Fig. 6 compile the occurrences for the different types of observed local intergranular corrosion behaviors. They are sorted according to GB type as derived from the morphology of the GBs at the topmost surface. It can be seen that all types of GBs except the Σ3 coherent twins show preferential reactivity compared to the adjacent grains. For the coherent twins, the absence of early intergranular corrosion is assigned to the intrinsic resistant character of these boundaries to intergranular corrosion. For low Σ CSLs (including Σ3 incoherent twins), full protection by the pre-adsorbed MBT layer was the only observed behavior, in agreement with the lower intrinsic reactivity expected for these boundaries compared to high Σ CSLs and random boundaries. In other words, the MBT layer pre-adsorbed in low Σ CSLs, i.e. before CV cycling in the Cu(I) oxidation range, is protective enough so that preferential intergranular electrochemical reactivity is completely inhibited. Whereas, in the high Σ CSLs and random boundaries, intergranular reactivity is only mitigated, because of the higher electrochemical reactivity of these boundaries and possibly because of the more defective character of the MBT layer pre-formed in these boundaries.

For the random GBs, characterized by curved morphologies at the topmost surface, protection against active dissolution by the accumulation of reaction products forming a protective film predominates protection by the pre-adsorbed MBT layer. This is consistent with more intense activity occurring initially in the GB region, as expected from the ill-defined crystallographic character of the random boundaries, and producing transiently the Cu(I) ions leading to the formation of corrosion products. A major part of the measured random GB sites show transient protection after repeated anodic polarization, showing the fragile protectiveness provided by the reaction products accumulated in the random GBs.

Fewer of the measured GB sites could be associated with the other types of GBs. For the high Σ CSLs, characterized by short straight segments, protection by a film of corrosion products is also observed but more concurrently with protection by the pre-adsorbed MBT layer, which suggests a lower initial reactivity of these GBs compared to most random GBs. A major part of the measured high Σ CSLs show stable or delayed protection by a film of corrosion products in contrast with the random GBs whose major part show transient protection, which suggests lower protectiveness of the film grown in the random grain boundaries.

Conclusions

ECSTM and cyclic voltammetry have been applied to characterize the inhibiting effects of MBT on the early stages of

intergranular corrosion of microcrystalline copper in a 10 mM HCl (aq) acid solution. CV analysis of the macroscopic electrochemical response showed that MBT efficiently inhibits the active dissolution of copper in the acid medium by shifting to higher potential the onset of anodic dissolution and markedly lowering its intensity in an overpotential window of 0.15–0.2 V, owing to pre-adsorption and formation of a protective surface layer before CV cycling.

ECSTM analysis of the local intergranular corrosion behavior showed that the Σ3 coherent twins do not react preferentially compared to grains, in agreement with their intrinsic resistant character to intergranular corrosion. Low Σ CSL was observed to be protected by the pre-adsorbed MBT layer against net preferential dissolution in the GB region. All high Σ CSLs and random GBs were observed to react preferentially compared to grains. For these intrinsically more reactive boundaries, net dissolution, mitigated by the MBT layer pre-formed before CV cycling, was observed concurrently with protection resulting from preferential formation of reaction products in the GB regions. This protective effect of accumulated corrosion products was observed to be stable, transient or delayed in the conditions of repeated anodic cycling applied to force dissolution. For the high Σ CSL boundaries, this protection effect was more stable upon repeated cycling. For the random boundaries, this protection effect is generally transient, which is assigned to the intrinsically more reactive character of such GBs, less effectively protected by the local formation of a film of reaction products.

Acknowledgments

This project has received funding from the European Research Council (ERC) under the European Union's Horizon 2020 research and innovation programme (Advanced Grant CIMNAS, Corrosion Initiation Mechanisms at the Nanometric or Atomic Scale. Grant agreement no. 741123).

ORCID

Sagar B. Sharma https://orcid.org/0000-0001-8118-7580
Vincent Maurice https://orcid.org/0000-0001-5222-9972
Philippe Marcus https://orcid.org/0000-0002-9140-0047

References

1. J. Mieluch and M. Smialowski, "The behaviour of grain boundaries in iron during anodic polarization in ammonium nitrate solution." *Corros. Sci.*, **4**, 237 (1964).
2. P. Lin, G. Palumbo, U. Erb, and K. T. Aust, "Influence of grain boundary character distribution on sensitization and intergranular corrosion of alloy 600." *Scripta Metallurgica et Materiala*, **33**, 1387 (1995).
3. A. Vinogradov, T. Mimaki, S. Hashimoto, and R. Z. Valiev, "On the corrosion behaviour of ultra-fine grain copper." *Scr. Mater.*, **41**, 316 (1999).
4. L. Lu, M. L. Sui, and K. Lu, "Superplastic extensibility of nanocrystalline copper at room temperature." *Science*, **287**, 1463 (2000).
5. V. Y. Gerrtsman and S. M. Gruemer, "Study of grain boundary character along intergranular stress corrosion crack paths in austenitic alloys." *Acta Mater.*, **49**, 1589 (2001).
6. S. H. Kim, U. Erb, K. T. Aust, and G. Palumbo, "Grain boundary character distribution and intergranular corrosion behavior in high purity aluminum." *Scr. Mater.*, **44**, 835 (2001).
7. H. Miyamoto, K. Yoshimura, T. Mimaki, and M. Yamashita, "Behavior of intergranular corrosion of ⟨011⟩ tilt grain boundaries of pure copper bicrystals." *Corros. Sci.*, **44**, 1835 (2002).
8. M. Shimada, H. Kokawa, Z. J. Wang, Y. S. Sato, and I. Karibe, "Optimization of grain boundary character distribution for intergranular corrosion resistant 304 stainless steel by twininduced grain boundary engineering." *Acta Mater.*, **50**, 2331 (2002).
9. E. M. Lehockey, A. M. Brennenstuhl, and I. Thompson, "On the relationship between grain boundary connectivity, coincident site lattice boundaries, and intergranular stress corrosion cracking." *Corros. Sci.*, **46**, 2383 (2004).
10. V. Randle, "'Special' boundaries and grain boundary plane engineering." *Scr. Mater.*, **54**, 1011 (2006).
11. S. Xia, B. Zhou, and W. Chen, "Effect of single-step strain and annealing on grain boundary character distribution and intergranular corrosion in Alloy 690." *J. Mater. Sci.*, **43**, 2990 (2008).
12. R. Jones and V. Randle, "Sensitisation behaviour of grain boundary engineered austenitic stainless steel." *Mater. Sci. Eng., A*, **527**, 4275 (2010).
13. K. D. Ralston and N. Birbilis, *Effect of Grain Size on Corrosion: A Review, Corrosion*, **66**, 075005 (2010).
14. C. L. Changliang, S. Xi, H. Li, T. G. Liu, B. X. Zhou, W. J. Chen, and N. Wang, "Improving the intergranular corrosion resistance of 304 stainless steel by grain boundary network control." *Corros. Sci.*, **53**, 1880 (2011).
15. C. Luo, X. Zhou, G. E. Thompson, and A. E. Hughes, "Observations of intergranular corrosion in AA2024-T351: the influence of grain stored energy." *Corros. Sci.*, **61**, 35 (2012).
16. S. Kumar, B. S. Sai Prasad, V. Kain, and J. Reddy, "Methods for making alloy 600 resistant to sensitization and intergranular corrosion." *Corros. Sci.*, **70**, 55 (2013).
17. Y. Takehara, H. Fujiwara, and H. Miyamoto, ""Special" to "general" transition of intergranular corrosion in Sigma 3{111} grain boundary with gradually changed misorientation." *Corros. Sci.*, **77**, 171 (2013).
18. A. Stratulat, J. A. Duff, T. J. Marrow, and T. James, "Grain boundary structure and intergranular stress corrosion crack initiation in high temperature water of a thermally sensitised austenitic stainless steel, observed in situ." *Corros. Sci.*, **85**, 428 (2014).
19. E. Martinez-Lombardia, Y. Gonzalez-Garcia, L. Lapeire, I. De Graeve, K. Verbeken, L. Kestens, J. Mol, and H. Terryn, "Scanning electrochemical microscopy to study the effect of crystallographic orientation on the electrochemical activity of pure copper." *Electrochim. Acta*, **116**, 89 (2014).
20. B. V. Mahesh and R. K. Singh Raman, "Role of nanostructure in electrochemical corrosion and high temperature oxidation: a review." *Metallic Materials Transactions A*, **45A**, 5799 (2014).
21. N. Srinivasan, V. Kain, N. Birbilis, K. V. Mani Krishna, S. Shekhawat, and I. Samajdar, "Near boundary gradient zone and sensitization control in austenitic stainless steel." *Corros. Sci.*, **100**, 544 (2015).
22. E. Martinez-Lombardia, L. Lapeire, V. Maurice, I. De Graeve, K. Verbeken, L. H. Klein, L. Kestens, P. Marcus, and H. Terryn, "In situ scanning tunneling microscopy study of the intergranular corrosion of copper." *Electrochem. Commun.*, **41**, 1 (2014).
23. E. Martinez-Lombardia, V. Maurice, L. Lapeire, I. De Graeve, K. Verbeken, L. H. Klein, L. Kestens, P. Marcus, and H. Terryn, "In situ scanning tunneling microscopy study of grain-dependent corrosion on microcrystalline copper." *J. Phys. Chem. C*, **118**, 25421 (2014).
24. H. Chen, V. Maurice, L. H. Klein, L. Lapeire, K. Verbeken, H. Terryn, and P. Marcus, "Grain boundary passivation studied by in situ scanning tunneling microscopy on microcrystalline copper." *J. Solid State Electrochem.*, **19**, 3501 (2015).
25. H. Chen, M. Bettayeb, V. Maurice, L. H. Klein, L. Lapeire, K. Verbeken, H. Terryn, and P. Marcus, "Local passivation of metals at grain boundaries: in situ scanning tunneling microscopy study on copper." *Corros. Sci.*, **111**, 659 (2016).
26. M. Bettayeb, V. Maurice, L. H. Klein, L. Lapeire, K. Verbeken, and P. Marcus, "Nanoscale intergranular corrosion and relation with grain boundary character as studied in situ on copper." *J. Electrochem. Soc.*, **165**, C835 (2018).
27. D. Chadwick and T. Hashemi, "Electron spectroscopy of corrosion inhibitors: surface film formed by 2-mercaptobenzothiazole and 2-mercaptobenzimidazole on copper." *Surf. Sci.*, **89**, 649 (1979).
28. M. Ohsawa and W. Suëtaka, "Spectro-electrochemical studies of the corrosion inhibition of copper by mercaptobenzothiazole." *Corros. Sci.*, **19**, 709 (1979).
29. J. C. Marconato, L. O. Bulboes, and M. L. Temperini, "A spectroelectrochemical study of the inhibition of the electrode process on copper by 2-mercaptobenzothiazole in ethanolic solutions." *Electrochim. Acta*, **43**, 771 (1998).
30. R. Woods, G. A. Hope, and K. Watling, "A SERS spectroelectrochemical investigation of the interaction of 2-mercaptobenzothiazole with copper, silver and gold surfaces." *J. Appl. Electrochem.*, **30**, 1209 (2000).
31. C. W. Yan, H. C. Lin, and C. N. Cao, "Investigation of inhibition of 2-mercaptobenzothiazole for copper corrosion." *Electrochim. Acta*, **45**, 2815 (2000).
32. M. Antonijevic and M. Petrovic Mihajlovic, "Copper corrosion inhibitors. a review." *Int. J. Electrochem. Sci.*, **3**1 (2008).
33. M. M. Antonijevic, S. M. Milic, and M. B. Petrovic, "Films formed on copper surface in chloride media in the presence of azoles." *Corros. Sci.*, **51**, 1228 (2009).
34. F. M. A. Kharafi, N. A. Al-Awadi, I. M. Ghayad, R. M. Abdullah, and M. R. Ibrahim, "Novel technique for the application of azole corrosion inhibitors on copper surface." *Mater. Trans.*, **51**, 1671 (2010).
35. G. Gece, "Drugs: a review of promising corrosion inhibitors." *Corros. Sci.*, **53**, 3873 (2011).
36. L. P. Kazansky, I. A. Selyaninov, and Y. I. Kuznetsov, "Adsorption of 2-mercaptobenzothiazole on copper surface from phosphate solutions." *Appl. Surf. Sci.*, **258**, 6807 (2012).
37. M. Finsgar and D. K. Merl, "An electrochemical, long-term immersion, and XPS study of 2-mercaptobenzothiazole as a copper corrosion inhibitor in chloride solution." *Corros. Sci.*, **83**, 64 (2014).
38. I. Milosev, N. Kovacevic, J. Kovac, and A. Kokalj, "The roles of mercapto, benzene and methyl groups in the corrosion inhibition of imidazoles on copper: I. experimental characterization." *Corros. Sci.*, **98**, 107 (2015).
39. M. Petrovic Mihajlovic and M. Antonijevic, "Copper corrosion inhibitors. period 2008-2014. a review." *Int. J. Electrochem. Sci.*, **10**1027 (2015).
40. Y.-H. Chen and A. Erbe, "The multiple roles of an organic corrosion inhibitor on copper investigated by a combination of electrochemistry-coupled optical in situ spectroscopies." *Corros. Sci.*, **145**, 232 (2018).
41. A. Fateh, M. Aliofkhazraei, and A. R. Rezvanian, "Review of corrosive environments for copper and its corrosion inhibitors." *Arabian J. Chem.*, **13**, 481 (2020).
42. T. Shahrabi, H. Tavakholi, and M. G. Hosseini, "Corrosion inhibition of copper in sulphuric acid by some nitrogen heterocyclic compounds." *Anti-Corrosion Methods and Materials*, **54**, 308 (2007).

43. Z. Zhang, Q. Wang, X. Wang, and L. Gao, "The influence of crystal faces on corrosion behavior of copper surface: first-principle and experiment study." *Appl. Surf. Sci.*, **396**, 746 (2017).
44. X. Wu, F. Wiame, V. Maurice, and P. Marcus, "Adsorption and thermal stability of 2-mercaptobenzothiazole corrosion inhibitor on metallic and pre-oxidized Cu(111) model surfaces." *Appl. Surf. Sci.*, **508**, 145132 (2020).
45. X. Wu, F. Wiame, V. Maurice, and P. Marcus, "2-Mercaptobenzothiazole corrosion inhibitor deposited at ultra-low pressure on model copper surfaces." *Corros. Sci.*, **166**, 108464 (2020).
46. X. Wu, F. Wiame, V. Maurice, and P. Marcus, "Moiré structure of 2-mercapto-benzothiazole corrosion inhibitor adsorbed on (111)-oriented copper surface." *J. Phys. Chem. C*, **124**, 15995 (2020).
47. E. Vernack, D. Costa, P. Tingaut, and P. Marcus, "DFT studies of 2-mercapto-benzothiazole and 2-mercaptobenzimidazole as corrosion inhibitors for copper." *Corros. Sci.*, **174**, 108840 (2020).
48. F. Chiter, D. Costa, V. Maurice, and P. Marcus, "DFT investigation of 2-mercaptobenzothiazole adsorption on model oxidized copper surfaces and relation-ship with corrosion inhibition." *Appl. Surf. Sci.*, **537**, 147802 (2021).
49. L. Lapeire, E. Martinez Lombardia, K. Verbeken, I. De Graeve, L. Kestens, and H. Terryn, "Effect of neighboring grains on the microscopic corrosion behavior of a grain in polycrystalline copper." *Corros. Sci.*, **67**, 179 (2013).
50. L. Lapeire, E. Martinez Lombardia, K. Verbeken, I. De Graeve, L. Kestens, and H. Terryn, "Structural dependence of gold deposition by nanoplating in polycrystal-line copper." *J. Mater. Sci.*, **49**, 3909 (2014).
51. D. Zuili, V. Maurice, and P. Marcus, "Surface structure of nickel in acid solution studied by in situ STM." *J. Electrochem. Soc.*, **147**, 1393 (2000).
52. A. Seyeux, V. Maurice, L. H. Klein, and P. Marcus, "In situ STM study of the initial stages of growth and of the structure of the passive film on Ni(111) in 1 mM NaOH (aq)." *J. Solid State Electrochem.*, **9**, 337 (2005).
53. A. Seyeux, V. Maurice, L. H. Klein, and P. Marcus, "In situ STM study of the effect of chloride on the growth mechanism and structure of the passive film on nickel in alkaline solution." *J. Electrochem. Soc.*, **153**, B453 (2006).
54. V. Maurice, L. H. Klein, H.-H. Strehblow, and P. Marcus, "In situ STM study of the surface structure, dissolution and early stages of electrochemical oxidation of the Ag(111) electrode." *J. Phys. Chem. C*, **111**, 16351 (2007).
55. N. Li, V. Maurice, L. H. Klein, and P. Marcus, "Structure and morphology modifications of silver surface in the early stages of sulphide growth in alkaline solution." *J. Phys. Chem. C*, **116**, 7062 (2012).
56. Gwyddion, "Free SPM (AFM, SNOM/NSOM, STM, MFM …) data analysis software." http://gwyddion.net/.
57. H.-H. Strehblow and B. Titze, "The investigation of the passive behaviour of copper in weakly acid and alkaline solutions and the examination of the passive film by Esca and ISS." *Electrochim. Acta*, **25**, 839 (1980).
58. Y. Feng, K. S. Siow, W. K. Teo, K. L. TanL, and A. K. Hsieh, "Corrosion mechanisms and products of copper in aqueous solutions at various pH values." *Corrosion*, **53**, 389 (1997).
59. B. Beverskog and I. Puigdomenech, *Pourbaix Diagrams for the System Copper-Chlorine at 5-100 C. SKI* (Swedish Nuclear Power Inspectorate (SKI)) SKI Rapport 98:19 (Nyköping) (1998).
60. O. Magnussen, L. Zitzler, B. Gleich, M. Vogt, and R. J. Behm, "In-situ atomic-scale studies of the mechanisms and dynamics of metal dissolution by high-speed STM." *Electrochim. Acta*, **46**, 3725 (2001).
61. M. Kruft, B. Wohlmann, C. Stuhlmann, and K. Wandelt, "Chloride adsorption on Cu(111) electrodes in dilute HCl solutions." *Surf. Sci.*, **377**, 601 (1997).
62. M. Vogt, A. Lachenwitzer, O. Magnussen, and R. J. Behm, "In-situ stm study of the initial stages of corrosion of Cu(100) electrodes in sulfuric and hydrochloric acid solution." *Surf. Sci.*, **399**, 49 (1998).
63. L.-J. Wan and K. Itaya, "In situ scanning tunneling microscopy of Cu(110): atomic structures of halide adlayers and anodic dissolution." *J. Electroanal. Chem.*, **473**, 10 (1999).
64. W. H. Li, Y. Wang, J. H. Ye, and S. F. Y. Li, "In situ STM study of chloride adsorption on Cu(110) electrode in hydrochloric acid aqueous solution." *J. Phys. Chem. B*, **105**, 1829 (2001).
65. T. Hai Phan, T. Kosmala, and K. Wandelt, "Potential dependence of self-assembled porphyrin layers on a Cu(111) electrode surface: in-situ STM study." *Surf. Sci.*, **631**, 207 (2015).
66. M. Bettayeb, V. Maurice, L. H. Klein, L. Lapeire, K. Verbeken, and P. Marcus, "Combined in situ microstructural study of the relationships between local grain boundary structure and passivation on microcrystalline copper." *Electrochim. Acta*, **305**, 240 (2019).